

Polymersomes: Tough Vesicles Made from Diblock Copolymers

Bohdana M. Discher,¹ You-Yeon Won,² David S. Ege,¹
James C-M. Lee,¹ Frank S. Bates,² Dennis E. Discher,^{1*}
Daniel A. Hammer^{1*}

Vesicles were made from amphiphilic diblock copolymers and characterized by micromanipulation. The average molecular weight of the specific polymer studied, polyethyleneoxide-polyethylene (EO₄₀-EE₃₇), is several times greater than that of typical phospholipids in natural membranes. Both the membrane bending and area expansion moduli of electroformed polymersomes (polymer-based liposomes) fell within the range of lipid membrane measurements, but the giant polymersomes proved to be almost an order of magnitude tougher and sustained far greater areal strain before rupture. The polymersome membrane was also at least 10 times less permeable to water than common phospholipid bilayers. The results suggest a new class of synthetic thin-shelled capsules based on block copolymer chemistry.

Amphiphilic block copolymers in water, like natural phospholipids, can self-assemble into various ordered mesophases (1–3), notably lamellar structures. The symmetry and stability of the microstructure depend intimately on chain size and chemistry as well as on physical variables such as temperature T . At dilute concentrations of natural amphiphiles in water, bilayer structures with a thickness of only a few nanometers can form; for cells, such membranes have permeability, stability, and mechanical characteristics that are central to function (3, 4). These characteristics also affect how liposomes and their complexes encapsulate and deliver active agents (5). Small amphiphiles of natural origin have inspired the engineering of higher molecular weight, synthetic analogs defined as superamphiphiles (6), which include linear diblock copolymers composed of a serial tandem of hydrophilic and hydrophobic chains. We report here some of the properties of membranes assembled from one such superamphiphile, polyethyleneoxide-polyethylene [EO₄₀-EE₃₇; number-average molecular weight $M_n \approx 3900$ g/mol (1, 7)]. This neutral, synthetic polymer has a mean contour length (~23 nm) about 10 times that of a typical phospholipid acyl chain (Fig. 1A). Chains of polyethyleneoxide (PEO), also referred to as polyethylene glycol (PEG), are also notable for imparting biocompatibility to membranes (8). The specific diblock copolymer studied here had previously been synthesized as one chain, designated OE-7, among a low polydis-

persity series with varied molecular weights and block size distributions (7); OE-7 was shown to have a robust propensity to form a lamellar phase in water over a broad range of concentrations and temperatures (25°C included) (1).

Small, nonaggregating vesicles (≤ 200 nm) assembled from OE-7 were first observed by cryogenic transmission electron microscopy (cryo-TEM) after hydration and preparative vitrification (Fig. 1B) (9). Worm-like micelles (2) as well as spherical micelles coexist with the vesicles. Imaging of the hydrophobic cores of these structures revealed a core thickness $d \approx 8$ nm, significantly greater than $d \approx 3$ nm for phospholipid bilayers (3). To facilitate detailed characterization of the material properties of block copolymer lamellae, we made giant vesicles (from 20 to 50 μm) of OE-7 by electroformation (10), a process in which a thin film of polymer on adjacent electrodes was phoresed by alternating current into aqueous solution. Thermal undulations of the quasi-spherical polymersome membranes provided an immediate indication of membrane softness (Fig. 2A). Furthermore, if the vesicles were made in the presence of either a 10-kD fluorescent dextran (Fig. 2B) or a protein such as globin, the probe was found to be readily encapsulated and retained by the vesicle for at least several days. The polymersomes further proved highly deformable and could be aspirated into micrometer-diameter pipettes (Fig. 2, C and D) (10).

The elastic behavior of a polymersome membrane in micropipette aspiration (at ~23°C) appeared comparable in quality to a fluid-phase lipid membrane. Analogous to a lipid bilayer, at low but increasing aspiration pressures, the thermally undulating polymersome membrane was progressively smoothed, increasing the projected area logarithmically

with tension, τ , (Fig. 3A). From the slope of this increase versus the fractional change, α , in vesicle area the bending modulus, K_b , was calculated (11)

$$K_b \approx k_B T \ln(\tau)/(8\pi\alpha) + \text{constant} \quad (1)$$

and found to be $1.4 \pm 0.3 \times 10^{-19}$ J (six vesicles) (k_B is Boltzmann's constant). Above a crossover tension, τ_x , a renormalized area expansion modulus (11), K_a , was obtained from the relation

$$K_a = \tau/\alpha \quad (2)$$

Aspiration in this regime primarily corresponds to a true—rather than a projected—reduction in molecular surface density, and for the polymersome membranes, $K_a = 120 \pm 20$ mN/m (21 vesicles). Fitted moduli were checked for each vesicle by verifying that the crossover tension, $\tau_x = (K_a/K_b)(k_B T/8\pi)$, suitably fell between appropriate high-tension (membrane stretching) and low-ten-

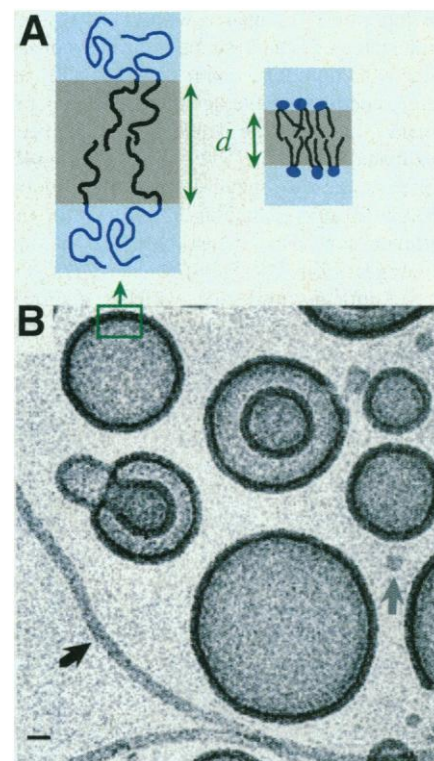


Fig. 1. Molecular assemblies and copolymer structures in water. (A) Schematic representation of diblock copolymer EO₄₀-EE₃₇, also designated OE-7, with chain structure

t-butyl-[CH₂-CH(C₂H₅)]₃₇-[CH₂-CH₂-O]₄₀-H. The number-average molecular weight is ~3900 g/mol. For a simple comparison of relative hydrophobic core thickness d , a bilayer of typical lipids (3) are schematically shown next to the assembly of copolymers. (B) Aqueous suspensions of OE-7 vesicles in dominant coexistence with rodlike (black arrow) and spherical (gray arrow) micelles. Observations were made by cryo-TEM (9); the scale bar at lower left is 20 nm and the mean lamellar thickness is ~8 nm.

¹School of Engineering and Applied Science, and Institute for Medicine and Engineering, University of Pennsylvania, Philadelphia, PA 19104, USA. ²Department of Chemical Engineering and Materials Science, University of Minnesota, Minneapolis, MN 55455, USA.

*To whom correspondence should be addressed.

REPORTS

sion (membrane smoothing) regimes. Measurements of both moduli, K_a and K_b , were further found to yield essentially unimodal distributions with small enough standard deviations ($\approx 20\%$ of mean) to be considered characteristic of unilamellar PEO-PEE vesicles. Interestingly, the moduli are also well within the range reported for various pure and mixed lipid membranes. SOPC (1-stearoyl-2-oleoyl phosphatidylcholine) in parallel manipulations was found, for example, to have $K_a \approx 180$ mN/m (Fig. 3B) and $K_b \approx 0.8 \times 10^{-19}$ J, which are largely identical to prior measures (4, 11). Lastly, at aspiration rates where projection lengthening was limited to < 1 $\mu\text{m/s}$, the microdeformation proved largely reversible, consistent again with an elastic response.

The measured K_a is most simply approximated by four times the surface tension, γ , of a pure hydrocarbon-water interface ($\gamma = 20$ to 50 mJ/m²) and thus reflects the summed cost of two monolayers in a bilayer (12). The softness of K_a compared with gel or crystalline states of lipid systems is further consistent with liquidlike chain disorder (13); indeed, because the average interfacial area per chain, $\langle A_c \rangle$, in the lamellar state has been estimated to be $\langle A_c \rangle \geq 2.5$ nm² per molecule (1), the root-mean-squared area fluctuations at any particular height within the bilayer can also be estimated to be, on average, $\langle \delta A_c^2 \rangle^{1/2} = (\langle A_c \rangle k_B T / K_a)^{1/2} \approx 0.3$ nm² per molecule, which is a significant fraction of $\langle A_c \rangle$ and certainly not small on a monomer scale. Moreover, presuming in the extreme, a bilayer of unconnected monolayers $d/2$ thick, with d estimated from cryo-TEM (Fig. 1), the PEE contour length is more than twice the monolayer core thickness and therefore configurationally mobile along its length. In addition, molecular theories (14) of chain packing in bilayers have suggested that, although at a fixed area per molecule there is a tendency for K_b to increase with

chain length (that is, membrane thickness), other factors such as large $\langle A_c \rangle$ can act to reduce K_b . Thus, despite the large chain size of OE-7, a value of K_b similar to that of lipid bilayers is not unduly surprising. Related to the length scales above, the root ratio of moduli, $(K_b/K_a)^{1/2}$, is generally recognized (3, 4, 14, 15) as providing a proportionate measure of membrane thickness. For the OE-7 membranes studied here, $(K_b/K_a)^{1/2} = 1.1$ nm on average. In comparison to fluid bilayer vesicles of phospholipids or phospholipids plus cholesterol, where the latter often have the highest K_a , it has been reported that $(K_b/K_a)^{1/2} \approx 0.53$ to 0.69 nm (11). A parsimonious continuum model for relating such a length scale to structure is based on the idea that the unconnected monolayers of the bilayer have, effectively, two stress-neutral surfaces located near each hydrophilic-hydrophobic core interface (15). If we assume that a membrane tension resultant may be located both above and below each interface, then

$$(K_b/K_a) = \delta_H \delta_C \quad (3)$$

where δ_H and δ_C are, respectively, distances from the neutral surfaces into the hydrophilic and hydrophobic cores. For lipid bilayers with $d/2 \approx 1.5$ nm and hydrophilic head groups 1 nm thick, estimates of $\delta_C \approx 0.75$ nm and $\delta_H \approx 0.5$ nm yield a root-product $[(\delta_H \delta_C)^{1/2} \approx 0.61$ nm], consistent with experimental results. The numerical result for PEO-PEE membranes (1.1 nm) suggests that the stress resultants are centered further from the interface, but not, perhaps surprisingly, in strict proportion to the increased thickness nor the polymer length.

Elastic behavior terminates in membrane rupture at a critical tension, τ_c , and areal strain, α_c . With lipids, invariably $\alpha_c \leq 0.05$, consistent, it appears, with a molecular theory of membranes under stress (16). For the polymersomes, cohesive failure occurred at $\alpha_c = 0.19 \pm 0.02$ (Fig. 3B). Another metric is the

toughness or cohesive energy density that, for such a fluid membrane, is taken as the integral of the tension with respect to areal strain, up to the point of failure:

$$E_c \approx \frac{1}{2} K_a \alpha_c^2 \quad (4)$$

For a range of natural phospholipids mixed with cholesterol, the toughness has been systematically measured, with E_c ranging from 0.05 to 0.5 mJ/m² (17). The OE-7 membranes, in comparison, are 5 to 50 times as tough, with $E_c \approx 2.2$ mJ/m². On a per molecule (18) rather than a per area basis, such critical energies are remarkably close to the thermal energy, $k_B T$, whereas such an energy density for lipid bilayers is a small fraction of $k_B T$. This difference indicates, for this relatively simple condensed matter system, the strong role that fluctuations in density must have in creating a lytic defect. Despite the comparative toughness of the polymersome membrane, a core "cavitation pressure," p_c , may be readily estimated as

Fig. 2. Giant unilamellar vesicles of EO₄₀-EE₃₇. (A) Vesicle immediately after electroformation; the membrane is seen to be thermally undulating. (B) Encapsulation of a 10-kD Texas Red-labeled dextran. (C and D) Microdeformation of a polymersome. The arrow marks the tip of an aspirated projection as it is pulled by negative pressure, ΔP , into the micropipette. Aspiration acts to (i) increase membrane tension, $\tau = \frac{1}{2} \Delta P R_p / (1 - R_p/R_s)$, where R_p and R_s are the respective radii of the micropipette and the outer spherical contour; and (ii) expand the original, projected vesicle surface area, A_0 , by the increment ΔA .

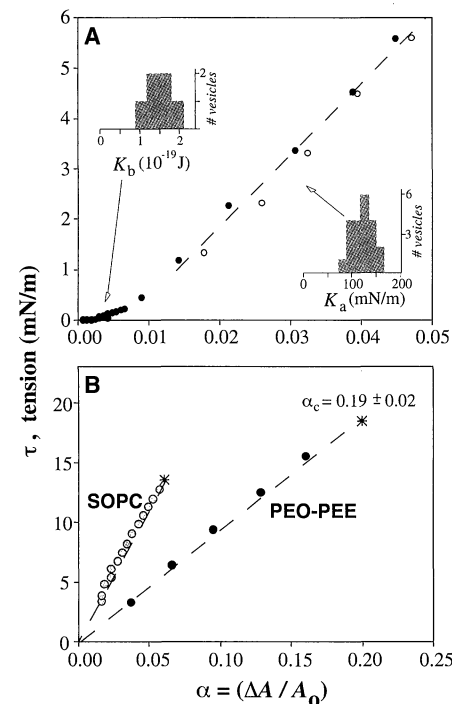
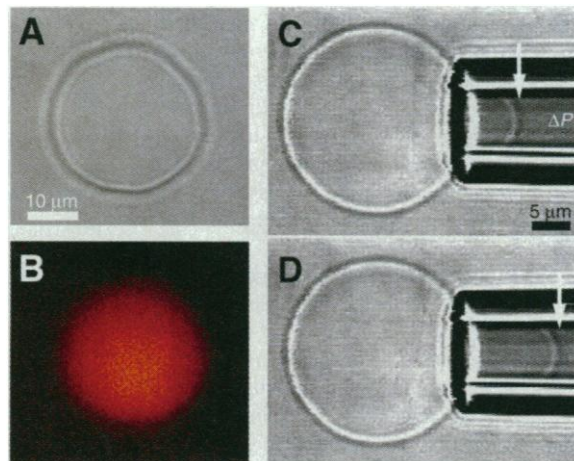


Fig. 3. Mechanical properties of polymersome membranes as assessed by micromanipulation. (A) Membrane elasticity revealed in membrane tension versus areal expansion. Filled circles indicate aspiration; open circles indicate graded release. The upper left inset shows the distribution of measurements for the bending modulus, K_b , as obtained from the initial phase of aspiration. The lower right inset shows the distribution of measurements for the area expansion modulus, K_a , as obtained from the linear phase of aspiration. (B) Membrane toughness determined by aspiration to the point of rupture (asterisk). For comparison, aspiration to the point of rupture of an electroformed SOPC lipid vesicle is also shown.

REPORTS

$$p_c = \tau_c/d \quad (5)$$

yielding a value of $p_c \approx -25$ atm, which falls in the middle of the range noted for lipid bilayers, $p_c \approx -10$ to -50 atm (4). Bulk liquids such as water and light organics are commonly reported to have measured tensile strengths of such a magnitude, as may be generically estimated from a ratio of nominal interfacial tensions to molecular dimensions (that is, $\sim\gamma/d$). In membrane systems, this analogy again suggests an important role for density fluctuations, which are manifested in a small K_a and which must become transversely correlated upon coalescing into a lytic defect.

Because the previous estimate for $\langle\delta A_c^2\rangle^{1/2}$ is clearly not small compared with the cross section of H_2O , a finite permeability of OE-7 membranes to water is to be expected. Polymersome permeability was obtained by monitoring the exponential decay in vesicle swelling as a response to a step change in external medium osmolarity (19). The permeability coefficient, P_f , was $2.5 \pm 1.2 \mu\text{m/s}$. In contrast, membranes composed purely of phospholipids with acyl chains ≤ 18 carbon atoms typically have permeabilities in the fluid state at least an order of magnitude greater (25 to $150 \mu\text{m/s}$) (4). The OE-7 polymersomes are thus significantly less permeable to water—a distinction that may prove useful in application. However, on a per area basis, polymersome membranes and phospholipid membranes (with comparable K_a) exhibit similar fluctuations in area. This leads us to postulate that the ratio of permeabilities largely reflects the relative probability for water diffusion across the membrane and decreases with relative core thickness as $\exp(-d_{\text{OE7}}/d_{\text{lipid}}) \approx e^{-8/3} = 0.07$, which is a value close to the measured ratio of permeabilities for polymersomes versus lipid vesicles.

Vesicle morphology could be tuned by adjusting the osmotic pressure external to freely suspended polymersomes. Starting with an osmotically deflated tubular vesicle (Fig. 4), stepwise dilution of the external

osmolarity leads to water permeation and swelling through a quasi-equilibrated sequence of pearled spheres, pears, and buds, to a final tensed state. After the initial pearling of the tubule, the growth of large spheres at the expense of small spheres—a form of Ostwald ripening—is evident. Such shape transformations of vesicle capsules, the simple red cell included, have generally been correlated with energetic costs or constraints imposed by vesicle area, the number of membrane molecules making up vesicle area, the volume enclosed by the vesicle, and the curvature elasticity of the membrane (20). More recent theoretical and experimental efforts on fluid lipid bilayers (21) have separated the curvature elasticity between a local, K_b -scaled Helfrich term that includes a spontaneous curvature c_0 and a more nonlocal, area-difference-elasticity term predicated on monolayer unconnectedness in spherical-topology vesicles. To oppose any relaxation of leaflet area difference, a lack of lipid transfer or “flip-flop” between layers must be postulated. Only with such a nonlocal term or $c_0 \neq 0$, it seems, can a vesicle maintain in apparent equilibrium the sorts of multisphere (21, 22) and budded morphologies observable in both lipid systems and in the osmotically deflated polymersomes. Because wormlike and spherical micelles are in evidence (Fig. 1B), $c_0 \neq 0$ appears likely. However, heterogeneity in the morphology of polymersomes, both small (Fig. 1B) and large (Fig. 4) vesicles, also suggests an important contribution from monolayer area difference, a process-dependent feature that arises upon vesicle closure (21).

Polymersomes, of the general type examined here, enable direct measurements of the material properties of lamellae and put to the test some basic ideas of membrane assembly. Compared with lipids, the increased length and conformational freedom of polymer chains not only provide a basis for enhanced toughness and reduced permeability of membranes but also suggest that the rich diversity of block copolymer chemistries (molecular weights, block fraction, block architecture)

portends a plethora of novel, artificial membranes. Additional control over membrane properties may be afforded, for example, through selective cross-linking of block copolymer hydrocarbon chains as demonstrated with wormlike micelles (2). As with the rich variety of phospholipids and membrane modifiers, each synthetic membrane might find its own application in transport, rheology, or encapsulation, rationally based on a suitable selection of material properties, thermal behaviors, and permeabilities.

References and Notes

1. D. A. Hajduk, M. B. Kossuth, M. A. Hillmyer, F. S. Bates, *J. Phys. Chem. B* **102**, 4269 (1998); H. E. Warriner, S. H. J. Idziak, N. L. Slack, P. Davidson, C. R. Safinya, *Science* **271**, 969 (1996); K. Yu and A. Eisenberg, *Macromolecules* **31**, 3509 (1998).
2. Y.-Y. Won, H. T. Davis, F. S. Bates, *Science* **283**, 960 (1999).
3. Reviewed in R. Lipowsky and E. Sackmann, Eds., *Structure and Dynamics of Membranes—From Cells to Vesicles*, vol. 1 of the *Handbook of Biological Physics* (Elsevier Science, Amsterdam, 1995). Note (as tabulated on page 19 of this reference) that for a generic plasma membrane such as that of the red blood cell, about three-fourths of the phospholipids have acyl chains of lengths 16, 18, or 20 carbon atoms. Note also (as indicated on pages 229 or 658 of the same reference) that a bilayer of lipids with chains of 16 or 18 carbon atoms in the biologically relevant disordered liquid phase (L_d) may be estimated to have a thickness $d \approx 3$ nm.
4. M. Bloom, E. Evans, O. G. Mouritsen, *Q. Rev. Biophys.* **24**, 293 (1991); D. Needham and D. Zhelev, in *Vesicles*, M. Rosoff, Ed. (Dekker, New York, 1996), chap. 9.
5. G. Cevc, in (3), chap. 9; D. D. Lasic, in (3), chap. 10; I. Koltover, T. Salditt, J. O. Radler, C. Safinya, *Science* **281**, 78 (1998); T. O. Harasym, P. R. Cullis, M. B. Bally, *Cancer Chemother. Pharmacol.* **40**, 309 (1997).
6. J. J. L. M. Cornelissen, M. Fischer, N. A. J. M. Sommerdijk, R. J. M. Nolte, *Science* **280**, 1427 (1998).
7. M. A. Hillmyer and F. S. Bates, *Macromolecules* **29**, 6994 (1996); M. A. Hillmyer et al., *Science* **271**, 976 (1996). For $\text{EO}_{40}\text{-EE}_{37}$, a polydispersity measure is given by $M_w/M_n \sim 1.10$, where M_w and M_n are the weight-average and number-average molecular weights, respectively. The PEO volume fraction is $f_{\text{EO}} = 0.39$.
8. J. M. Harris and S. Zalipsky, Eds., *Poly(ethylene glycol): Chemistry and Biological Applications* (American Chemical Society, Washington, DC, 1997). Also, as reviewed in D. D. Lasic, in (3), chap. 10, PEG chain lengths that optimize the stealth of liposomes, that is, lipid-conjugated PEG leading to the longest blood circulation time of liposomes, are in the approximate range of EO_{34} to EO_{114} .
9. Thin (about 10- to 300-nm) films of aqueous solution suspended in a microperforated grid were prepared in an isolated chamber with temperature and humidity control. The sample assembly was rapidly vitrified with liquid ethane at its melting temperature (~ 90 K), and this was kept under liquid nitrogen until it was loaded onto a cryogenic sample holder (Gatan 626). We obtained images with a JEOL 1210 at 120 kV using a nominal underfocus of $6 \mu\text{m}$ and digital recording. For a more detailed description or related examples, see Z. Lin, M. He, L. E. Scriven, H. T. Davis, *J. Phys. Chem.* **97**, 3571 (1993); A. Walter, P. K. Vinson, A. Kaplun, Y. Talmon, *Biophys. J.* **60**, 1315 (1991).
10. $\text{EO}_{40}\text{-EE}_{37}$, synthesized by a combination of anionic polymerization and catalytic hydrogenation, was subsequently lyophilized into a solid and solubilized, when needed, in chloroform at 4 mg/ml. Evaporation of the solvent under nitrogen followed by vacuum drying for 3 to 48 hours was used to deposit a film on 1-mm-diameter platinum wire electrodes held in a Teflon frame (5 mm separation). The Teflon frame and electrodes were assembled into a chamber by

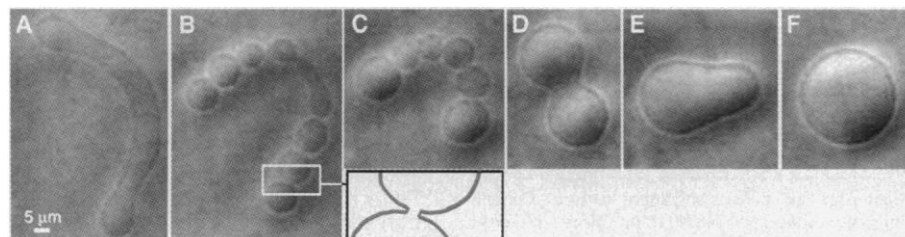


Fig. 4. Shape transformations driven by osmotic swelling of a single polymersome and imaged in phase contrast video microscopy. The vesicle was formed in 100 mOsm sucrose, and the external sucrose solution was progressively diluted with distilled water from ~ 150 mOsm glucose over a period of 90 min. The state in (A) is a giant tubular state that swells with the initial appearance (B) of interconnected spheres (inset) that conserve vesicle topology. This is followed by coalescence and disappearance (C to E) of the spheres before final transformation to a single, tensed sphere (F).

The Formation of Jupiter's Faint Rings

Joseph A. Burns,^{1*} Mark R. Showalter,² Douglas P. Hamilton,³
Philip D. Nicholson,¹ Imke de Pater,⁴ Maureen E. Ockert-Bell,¹
Peter C. Thomas¹

Observations by the Galileo spacecraft and the Keck telescope showed that Jupiter's outermost (gossamer) ring is actually two rings circumscribed by the orbits of the small satellites Amalthea and Thebe. The gossamer rings' unique morphology—especially the rectangular end profiles at the satellite's orbit and the enhanced intensities along the top and bottom edges of the rings—can be explained by collisional ejecta lost from the inclined satellites. The ejecta evolves inward under Poynting-Robertson drag. This mechanism may also explain the origin of Jupiter's main ring and suggests that faint rings may accompany all small inner satellites of the other jovian planets.

The well-known, opaque rings of Saturn and Uranus are populated primarily by centimeter- to meter-sized particles. In addition, all four giant planets have extensive but much more tenuous rings (1, 2) containing mainly micrometer-sized particles. Because particle collisions are unimportant in such rarified systems and because small grains are substantially perturbed by nongravitational forces, these ethereal rings provide valuable dynamical counterpoints to the dense, collisionally dominated systems.

Jupiter's rings—the archetype of ethereal ring systems—have three components (3): a main ring, an inner halo, and an outer gossamer ring. The main ring of normal optical depth $\tau \sim 10^{-6}$ and thickness <30 km extends radially inward about 6000 km (jovian radius = 71,398 km) from the orbit of the tiny moon Adrastea, with a dip in brightness of 20 to 30% around Metis's orbit (Table 1). Immediately interior to the main ring is the halo, a $\sim 10^4$ -km-thick and $\sim 2 \times 10^4$ -km-wide torus of dust, with τ comparable to the main ring. Exterior to the main ring lies the broad, fainter gossamer ring, with $\tau \sim 10^{-7}$, whose inner portion was observed in one Voyager image (4).

The ring system's structure was confirmed and refined through images obtained by the Galileo spacecraft (5) and the Keck 10-m telescope (6). The gossamer ring is actually two distinct, fairly uniform rings (Fig. 1, A and B). The brighter and narrower (Amalthea) ring is visible stretching radially outward from the main ring to the satellite Amalthea's orbit at 181,350 km. The fainter

and wider (Thebe) ring is terminated at the satellite Thebe's orbit (221,900 km). Some very diffuse material, which we refer to as the exterior gossamer material, seems to reach past Thebe, to perhaps 265,000 km.

As seen in these almost edge-on images, Jupiter's gossamer rings have a unique form. At their ansae, both rings have cross sections that are approximately rectangular, unlike the elliptical ends typically noted in images of thin, flat equatorial rings. As measured near the ansae, the half-thicknesses T of the gossamer rings are ~ 1300 km [inclination (i) = 0.41°] for the Amalthea ring and ~ 4400 km ($i = 1.14^\circ$) for the Thebe ring, with uncertainties of ± 100 km ($\pm 0.03^\circ$). These values are similar to the maximum excursions of the satellites associated with these rings from Jupiter's equatorial plane [1160 and 4310 km, respectively, with errors of ± 150 km (7)]. In addition, the radial excursions of the source satellites, as defined by their orbital eccentricities, seem to determine the radial decrease in brightness at the ansae of both rings (see crosses in Fig. 1A).

The ring's upper and lower edges are much brighter than their central cores (Fig. 1A), suggesting that the ring material is concentrated near the edges. Furthermore, the height (off the equatorial plane) of the peak brightness in each gossamer ring decreases linearly with projected radius as does the ring's total vertical extent in backscattered light (6). A similar banded appearance was inferred for the distribution of interplanetary dust particles (IDPs) from Infrared Astronomical Satellite scans of the zodiacal light (8). The cause is likely the same: a swarm of orbiting particles, with similar inclinations but random node orientations, that spend more time at their vertical turning points above and below the ecliptic (interplanetary case) or equatorial (jovian case) plane.

In the Voyager discovery image (4) and in two early Galileo frames (5), the Amalthea ring brightens by tens of percent with smaller scat-

sealing with coverslips, and this was subsequently filled with 100 mM sucrose solution. To begin generating vesicles from the film, we applied an alternating electric field to the electrodes (10 Hz, 10 V) while the chamber was mounted and viewed on the stage of an inverted microscope. Giant vesicles attached to the film-coated electrode were visible after 15 to 60 min. These were dissociated from the electrodes by lowering the frequency to 3 to 5 Hz for at least 15 min. The electroformation method is adapted from that of M. I. Angelova, S. Soleau, P. Meleard, J. F. Faucon, and P. Bothorel [*Prog. Coll. Polm. Sci.* **89**, 127 (1992)], as previously used by M. L. Longo, A. J. Waring, and D. A. Hammer [*Biophys. J.* **73**, 1430 (1997)]. The vesicles were stable for at least several days when kept sealed from air in a gas-tight, plastic syringe. Of additional note, vesicles were stable when resuspended in physiological saline at temperatures ranging from 10° to 50°C. Micromanipulation was done with micropipette systems analogous to those described by M. L. Longo *et al.* and D. E. Discher, N. Mohandas, and E. A. Evans [*Science* **266**, 1032 (1994)].

11. E. Evans and W. Rawicz, *Phys. Rev. Lett.* **64**, 2094 (1990); W. Helfrich and R.-M. Servuss, *Nuovo Cimento* **D3**, 137 (1984). Note that K_c did not differ by more than 10 to 20% from its nonrenormalized value.
12. J. Israelachvili, *Intermolecular and Surface Forces* (Academic Press, New York, ed. 2, 1991).
13. E. Evans and D. Needham, *J. Phys. Chem.* **91**, 4219 (1987).
14. I. Szleifer, D. Kramer, A. Ben-Shaul, D. Roux, W. M. Gelbart, *Phys. Rev. Lett.* **60**, 1966 (1988); A. Ben-Shaul, in (3), chap. 7.
15. A. G. Petrov and J. Bivas, *Prog. Surf. Sci.* **18**, 359 (1984).
16. R. R. Netz and M. Schick, *Phys. Rev. E* **53**, 3875 (1996). In this reference, the self-consistent calculation models lipids as nearly symmetric diblock copolymers, which are clearly closer in form to the molecules of this study.
17. D. Needham and R. S. Nunn, *Biophys. J.* **58**, 997 (1990).
18. Because the average interfacial area per chain, $\langle A_c \rangle$, in the lamellar state has been estimated to be $\langle A_c \rangle \approx 2.5 \text{ nm}^2$ per molecule, one estimates that $E_c \approx 1.3 k_B T$.
19. Vesicles were prepared in 100 mOsm sucrose solution, which established an initial, internal osmolarity. They were then suspended in an open-edge chamber formed between cover slips and containing 100 mOsm glucose. A single vesicle was aspirated with a suction pressure sufficient to smooth membrane fluctuations; the pressure was then lowered to a small holding pressure. With a second, transfer pipette, the vesicle was moved to a second chamber with 120 mOsm glucose. Water flows out of the vesicle due to the osmotic gradient between inside and outside, which leads to an increased projection length that is monitored over time. The exponential decrease in vesicle volume was calculated from video images and then fit to determine the permeability coefficient (P_f) (4). For reference, $P_f = 23.5 \pm 1.7 \mu\text{m/s}$ for SOPC from this method.
20. H. J. Deuling and W. Helfrich, *J. Phys.* **37**, 1335 (1976); S. Svetina and B. Zeks, *Eur. Biophys.* **17**, 101 (1989); U. Seifert, K. Berndl, R. Lipowsky, *Phys. Rev. A* **44**, 1182 (1991).
21. U. Seifert and R. Lipowsky, in (3), chap. 8; H.-G. Dobreiner, E. Evans, M. Kraus, U. Seifert, M. Wortis, *Phys. Rev. E* **55**, 4458 (1997).
22. S. Chaieb and S. Rica, *Phys. Rev. E* **58**, 7733 (1998).
23. We thank E. A. Evans, D. Needham, P. Nelson, and T. Lubensky for discussions. Support was primarily provided by the NSF-supported Materials Research Science and Engineering Center (MRSEC) at the University of Pennsylvania (DMR96-32598) and both the Center for Interfacial Engineering (CIE) and the MRSEC (DMR 98-09364) at the University of Minnesota. The work was also supported in part by grants from the Whitaker Foundation (D.D.) and National Institutes of Health [R01-HL62352-01(D.D.) and P01-HL8208 (D.H.)].

27 January 1999; accepted 5 April 1999

¹Center for Radiophysics and Space Research, Cornell University, Ithaca, NY 14853, USA. ²Space, Telecommunications and Radioscience Laboratory, Stanford University, Stanford, CA 94305, USA. ³Department of Astronomy, University of Maryland, College Park, MD 20742, USA. ⁴Department of Astronomy, University of California, Berkeley, CA 94720, USA.

*To whom correspondence should be addressed. E-mail: jab16@cornell.edu